energies

MDPI

Article

Design and Transient Analysis of a Natural Gas-Assisted Solar LCPV/T Trigeneration System

Yang Liu, Han Yue, Na Wang, Heng Zhang * and Haiping Chen

School of Energy, Power and Mechanical Engineering, North China Electric Power University, Beijing 102206, China; npmliuyang@ncepu.edu.cn (Y.L.); 120202202115@ncepu.edu.cn (H.Y.); NaWang@ncepu.edu.cn (N.W.); hdchenhaiping@163.com (H.C.)

* Correspondence: zhangchongheng@hotmail.com; Tel.: +86-185-1014-6466

Received: 27 September 2020; Accepted: 11 November 2020; Published: 13 November 2020

Abstract: This paper proposes a natural gas assisted solar low-concentrating photovoltaic/thermal trigeneration (NG-LCPV/T-TG) system. This novel system simultaneously provides electrical, thermal and cooling energy to the user. The design and dynamic simulation performance of the NG-LCPV/T-TG system is completed using Transient System Simulation (TRNSYS) software. The results show that the system can satisfy the requirements of the cooling and heating load. The proposed system maintains the experimental room temperature at about 25 °C under the cooling mode, at about 20 °C under the heating mode. The electrical and thermal energy produced by the low-concentrating photovoltaic/thermal (LCPV/T) system are 3819 kWh and 18,374 kWh. Meanwhile, the maximum coefficient of performance (COP) of the low temperature heat pump (LHP), high temperature heat pump (HHP) and chiller are 5, 2.2 and 0.6, respectively. This proposed system realizes the coupling of natural gas and solar energy in a building. In summary, this trigeneration system is feasible and it promotes the implementation of building integrated high-efficiency energy supply system.

Keywords: LCPV/T system; trigeneration system; natural gas; TRNSYS

1. Introduction

There is no doubt that China is the country with the highest energy consumption in the world. Unlike other countries with slow energy growth, China's energy growth accelerated in 2019 [1]. Within this growth, the proportion of coal consumption showed a downward trend, while the total consumption of renewable energy continued to increase [2].

However, the utilization of renewable energy was restricted by environmental and technological factors. Therefore, a complementary system of non-renewable energy and renewable energy came into being [3]. Additionally, solar energy is a clean and inexhaustible renewable energy, while natural gas is a non-renewable energy with the characteristics of high calorific value, convenient transportation, stable and continuous [4,5]. In the early and mid 21st century, the combination of solar energy and natural gas has been listed as the development goal of solar thermal utilization [6].

The concentrating solar photovoltaic/thermal (CPV/T) system uses water as a circulating cooling medium. The cooling water reduces the working temperature of photovoltaic (PV) cells and improves photovoltaic conversion efficiency [7]. The CPV/T system significantly improves the comprehensive utilization rate of solar energy and realizes high efficient power generation [8]. Due to the concentrator, the efficiency of the CPV/T system is higher than that of the conventional PV/T system. In particular, the thermal and electrical efficiency of the LCPV/T system has been shown to reach 54.48% and 14.49%, respectively [9]. Haiping Chen et al. designed a distributed compound parabolic concentrator (WD-CPC). The result showed that the light uniformity value was 0.153, which decreased the light non-uniformity about 0.13 or less compared with the flat-plate compound parabolic concentrator [10].

T. T. Chow focused on the development trend of the PV/T hybrid solar technology. In this framework, a review about the type and potential of PV/T technology was reported [11]. Moreover, Heng Zhang et al. proposed a LCPV/T system which included a low-concentrating compound parabolic concentrator. A baffle heat exchanger channel was applied to decrease the temperature of the PV cells. The thermal efficiency reached 55.11%, while the electrical efficiency reached 12.50% [12]. Guiqiang Li et al. established a model of PV/T system with static miniature solar concentrator. The simulated result and the experimental result were consistent. Compared with the flat plate PV/T system, the heat loss coefficient of the proposed system was lower [13]. Zexin Wang et al. designed a hybrid CPV/T system based on an unsteady-state thermal model. The result of the model was almost the same as the experimental output of the system. The thermal efficiency of the unsteady-state thermal model was 55.3%, and the measurement was 55.8% [14]. Bennett K. Widyolar et al. proposed a hybrid CPV/T system applied gallium arsenide solar cells. The simulated and experimental result showed that the exergy efficiency of the PV/T system could reach 37% when the thermal absorber ran at 500 °C [15].

Ramos A et al. [16] proposed a hybrid PV/T system for which the overall efficiency was above 70%, the electrical efficiency was 15–20%, and the thermal efficiency could exceed 50%. After reasonable design of combining with heat pump or chiller, the hybrid PV/T system could satisfy more than 60% of the heating demand and 50% of the cooling demand of urban households. In addition, Ramos A simulated the specific requirements of Seville, Rome, Madrid and Bucharest in a TRNSYS environment. The results showed that the PV/T system satisfied 60% of the heating demand and almost all of the cooling demand. The cost of this system achieved 30–40% lower than the equivalent pure photovoltaic system. Moreover, Braun R et al. [17] applied PV/T collectors as a heat source and heat sink for a reversible heat pump. Compared with traditional solar cooling system which used a reversible air-water heat pump as a cold or heat source, the overall efficiency and economic efficiency of this system were improved due to the reduction of electricity consumption for heat rejection. The auxiliary energy for this system was electricity from the grid. Bosheng Su et al. [18] proposed a novel combined cooling, heating and power system that could realize independent control of temperature and humidity. Compared with the traditional vapor compression air conditioning system, this novel system saved 50.41% of electrical energy when the same amount of cooling energy was generated.

In fact, only the CPV/T system cannot satisfy the demand of the user throughout a year. The main reason for this is the random fluctuation and intermittency of solar energy. To make up for the shortage, the CPV/T system needs to be combined with other stable energy supply systems [19]. As the most important fossil fuel, natural gas has the advantages of high calorific value and convenient transportation. Natural gas has been applied in distributed systems complementary to solar energy, such as the single-effect absorption air-conditioning system that used solar energy and natural gas as heat sources to provide heating and cooling to villas [20], the solar-natural gas household heating system that formed by the solar hot water system and natural gas wall-hung boiler system combined in series [21], and power generation system of solar energy combined with natural gas [22]. Francesco Calise et al. [23] analyzed the performance of a trigeneration system which consisted of CPV/T, biomass heater, single-effect absorption chiller and multi-effect distillation system. The exergy, economic and environmental performance of such system was studied in a TRNSYS environment. The results showed that the exergy destruction and exergy output increased with the increase of the PV/T area. Ighball Baniasad Askari et al. [24] studied and compared the economic performance of two kinds of solar systems that provided electricity, space cooling and domestic hot water. Recently, Christos Tzivanidis et al. [25] compared the performance of three different parabolic trough solar collectors (PTC) poly-generation systems. The energy efficiency of these three systems were 78.17%, 43.30% and 37.45%, respectively. The exergy efficiencies were 15.94%, 13.08% and 12.25%, respectively. Moreover, the payback times were 5.62 years, 7.82 years and 8.49 years, respectively. In particular, Zhang Heng et al. [26] proposed and analyzed a novel LCPV/T system which combined with absorption chiller. The inlet temperature, cooling water flow rate and refrigerant water flow rate influenced the cooling capacity of the chiller. The average COP of the chiller was 0.52. Furthermore, a LCPV/T

triple-generation system was proposed by Liu Yang et al. [27]. This system could produce hot water at 45–90 °C. Meanwhile, the electrical efficiency of the LCPV/T system was approximately 10%. The COP of the single-effect lithium bromide absorption chiller was above 0.5. To summarize, there are few studies on the dynamic characteristics of the trigeneration system that based on a CPV/T system and natural gas.

As discussed above, the trigeneration system has attracted the attention of a lot of scientists. However, research on the multi-source complementary system combining CPV/T technology with natural gas is extremely scarce. Therefore, this paper proposed a NG-LCPV/T-TG system in a TRNSYS environment. The electrical and thermal energy are produced by the LCPV/T system. This system uses different heat pumps as a primary auxiliary device and natural gas heater as a secondary auxiliary device. A novel form of energy cascade utilization is proposed in this paper. In addition, this system achieves a balance between supply and demand according to the requirements of the building. The temperature of the experimental room was controlled at 20 °C in winter and 25 °C in summer. Subsequently, the COP value of each equipment was improved. This research not only proposes a new energy utilization method, but also proves the feasibility of this novel system by one-year data. In particular, this research has a crucial effect on the promoting the comprehensive utilization of traditional energy and renewable energy.

2. System Layout

2.1. Systems Description

A design and transient analysis of the NG-LCPV/T-TG system is carried out by TRNSYS software [28]. The proposed system is based on the previous research of the LCPV/T triple-generation system [27], adding an auxiliary natural gas heater to ensure the indoor temperature stable. In particular, the proposed model could simultaneously satisfy the demands of space cooling and heating, electricity, and domestic hot water. In order to simulate the dynamic characteristics of the proposed system throughout one year, the local weather condition needs to be determined. The location selected is Beijing (40°09′33″ N, 116°31′47″ E), China. The building module is established using TRNBUILD in TRNSYS software.

In particular, the proposed system is based on an LCPV/T system. The simplified layout of the NG-LCPV/T-TG system is depicted in Figure 1. Moreover, there are two water source heat pumps in the proposed model: a low-temperature water source heat pump (LHP) using for space heating and a high-temperature water source heat pump (HHP) using for space cooling. For cooling purposes, a single-effect absorption lithium bromide chiller is adopted. Additionally, the capillary net system is used as the heat dissipation terminal. The electricity produced by the LCPV/T module is stored in the accumulator, which is used by the user or connected to the grid.

2.2. Operating Principle

The operating principle of this trigeneration system is briefly described as follows. The LCPV/T modules is applied as the main heat source. In addition, a natural gas heater and heat pumps are applied for auxiliary thermal energy, and the absorption chiller is used to achieve cooling energy. The operation control is based on two parameters. The temperature of the experimental room is the first parameter, which is the basic parameter to control the starting and stopping of the trigeneration system. The second parameter is the temperature of storage tank 1. In order to maintain the temperature comfortable, the room temperature is set according to the design manual. During winter, the room temperature is maintained at 20 °C. When the room temperature is below 20 °C, the heating mode is opened. Likewise, the room temperature is maintained at 25 °C in summer. Similar to the heating mode, when the room temperature is above 25 °C, the cooling mode is opened.

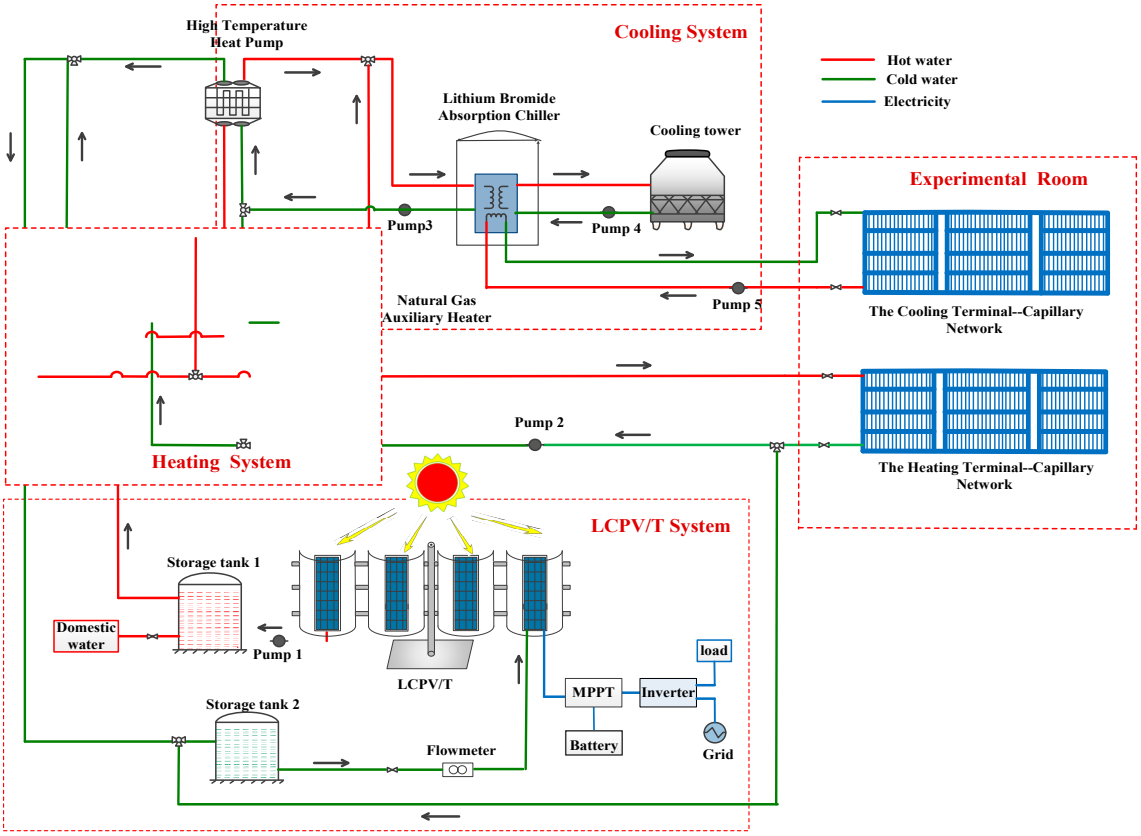

Figure 1. The configuration of the natural gas-assisted solar low-concentrating photovoltaic/thermal trigeneration (NG-LCPV/T-TG) system.

The temperature of storage tank 1 determines which device to use as a heat source for heating or cooling.

1. The schematic diagram of the NG-LCPV/T-TG in heating model is demonstrated in Figure 2. Loop 1, called the direct supply mode, is the cycle of NG-LCPV/T-TG system when the temperature of storage tank 1 is greater than or equal to 40 °C. This mode directly uses LCPV/T system as the heat source for space heating. When the temperature of storage tank 1 is below 40 °C but greater than 15 °C, the loop 2 mode is adopted. In loop 2, the outlet water of LCPV/T is used as the heat source of the LHP. This operational mode of loop 2 improves the comprehensive utilization efficiency of LCPV/T system, and the COP of LHP. Finally, when the temperature of storage tank 1 is below 15 °C, a natural gas auxiliary heater (NGAH) is used as the auxiliary heat source. In loop 3, LCPV/T system and LHP are all closed, only natural gas is used for space heating.

2. The schematic diagram of the NG-LCPV/T-TG in cooling model is demonstrated in Figure 3. When the temperature of storage tank 1 is greater than 40 °C, the loop 1 mode is adopted. In loop 1, the storage tank 1 is the heat source of the HHP. The HHP can provide hot water about 90 °C to the single-effect absorption lithium bromide chiller. When the temperature of the storage tank 1 is less than 40 °C, the natural gas auxiliary (NGAC) is used as the heat source of the lithium bromide chiller.

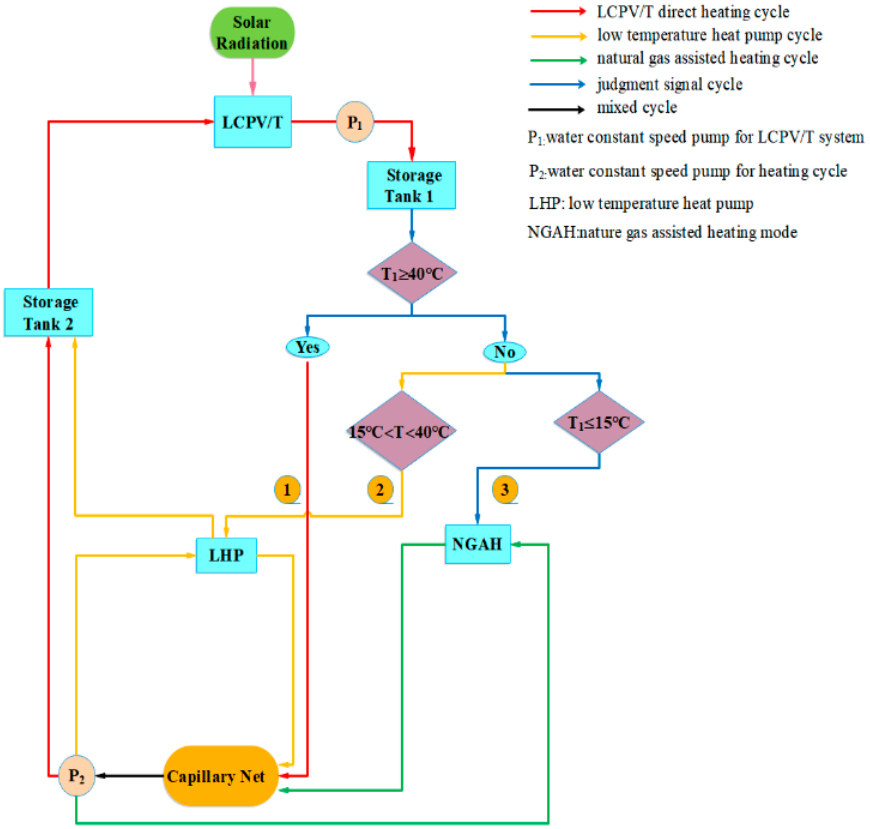

Figure 2. Schematic diagram of the NG-LCPV/T-TG system heating mode.

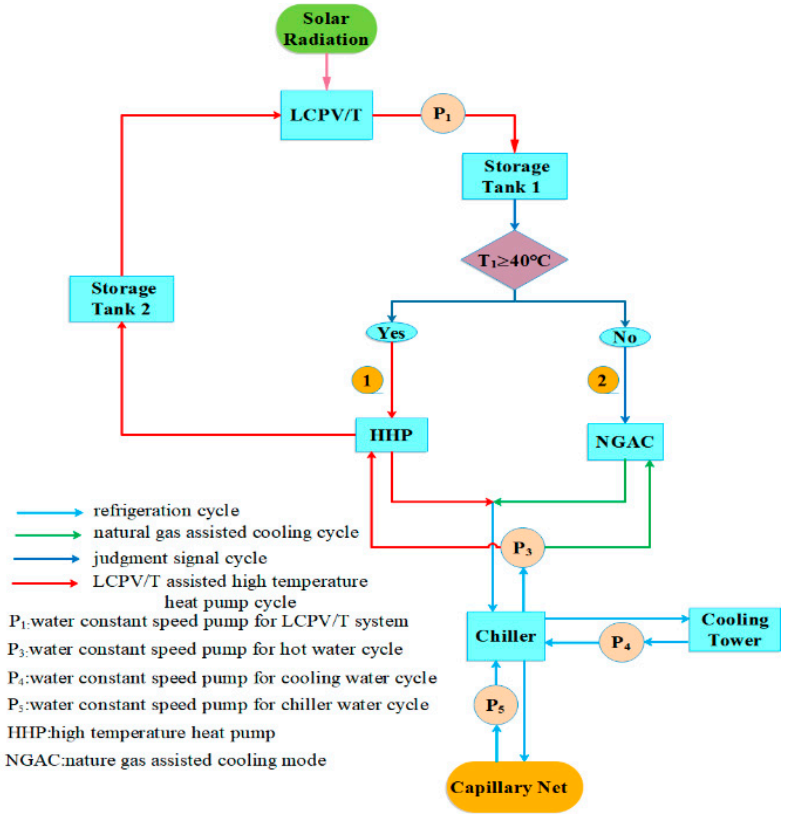

Figure 3. Schematic diagram of the NG-LCPV/T-TG system in cooling mode.

3. When neither space heating nor space cooling is needed, the trigeneration system provides domestic hot water.

3. Simulation Model

The main components of the proposed NG-LCPV/T-TG system are listed in Table 1. Table 1 lists the corresponding modules in TRNSYS software and briefly describes the equipment. All the components are implemented in the TRNSYS environment. In particular, the design parameters in the proposed system are set according to the previous experimental work [27].

Table 1. Depiction of main components.

Component	TRNSYS Model	Depiction
Building	Type 56	Experimental room.
LCPV/T	Type 50	A low-concentrating photovoltaic/thermal system
LHP	Type 225 [29]	An LHP that providing 40–45 °C hot water for space heating
HHP	Type 225 [29]	An HHP that providing 85–90 °C hot water for space cooling
Chiller	Type 107	A single-stage lithium bromide absorption chiller for which the thermal source comes from the HHP is used for space cooling
Cooling tower	Type 51b	The cooling tower is used to cool the water vapor in the condenser of the lithium bromide refrigerator
NGAH	Type 6	A natural gas auxiliary heater used to produce the hot water for space heating when the tank 1 temperature is below 15 °C
NGAC	Type 6	A natural gas auxiliary heater used to produce hot water for space cooling when the tank 1 temperature is below 40 °C
Pumps	Type 114	Fixed-volume pumps for space heating, cooling and domestic hot water circulation
Storage tank 1	Type 4	Thermal storage tank that stores the hot water which flew from the LCPV/T system
Storage tank 2	Type 4	Thermal storage tank that stores the cold water circulating from the cooling /heating system, at the same time use it as the source of the LCPVT system
Room temperature controller	Type 108	A Module that can control the cooling or heating mode of the experimental room
controller	Type 2	The on/off differential controller generates that can control the on/off of devices in the proposed system

3.1. Building Model

The experimental room was built using TRNBUILD in TRNSYS software. In addition, the capillary net is laid on the wall as the heat dissipation terminal. The detailed design parameters of the experimental room are listed in Table 2. The cooling and heat load of one year are calculated by the TRNSYS software. Moreover, the start and stop of equipment in the system are controlled based on the feedback of the temperature of the experimental room. As described above, the results simulated by the building model are closer to the actual test value.

Table 2. Depiction of the experimental room.

Parameter	Value	Unit
External wall area	11.76	m^2
Heat transfer coefficient of external wall	2.815	$W/(m^2 \cdot °C)$
Inner wall area	25.2	m^2
Heat transfer coefficient of inner wall (glass curtain wall)	4.0	$W/(m^2 \cdot °C)$
Capillary net area	33	m^2
Heat transfer coefficient of capillary net	0.227	$W/(m^2 \cdot °C)$
Ground area	37.8	m^2
Heat transfer coefficient of ground	0.313	$W/(m^2 \cdot °C)$
Density of air	1.204	kg/m^3
Specific heat of air	1012	$J/(kg \cdot °C)$
Pressure of air	101,325	Pa
External window area	4.5	m^2
Heat transfer coefficient of external window	5.68	$W/(m^2 \cdot °C)$
Shading factor of external window	0.20	-
Power of Computer	300	W
Amount of computer	4	-
People load	130	W/person
Number of persons	3	-

3.2. LCPV/T Model

In the proposed system, the parameters of each LCPV/T modules are listed in Table 3. Each group of LCPV/T module is composed of four photovoltaic (PV) cells. The cooling channels of the PV cells are connected in series. To ensure the supply of the heat and the flow, six groups of LCPV/T modules are connected in parallel. In particular, a dual-axis tracking mode is applied in the proposed system.

Table 3. Depiction of the low-concentrating photovoltaic/thermal (LCPV/T) model.

Parameter	Value	Unit
PV/T area	0.97344	m^2
PV/T fin efficiency factor	0.96	-
Fluid thermal capacitance	4190	$J/(kg \cdot °C)$
PV/T plate absorption	0.92	-
Number of glass covers	1	-
PV/T plate emittance	0.09	-
Loss coefficient for bottom and edge losses	0.3	$W/(m^2 \ °C)$
Transmittance absorbtance product	0.9	-
Temperature coefficient of PV cell	0.0032	1/°C
Temperature for cell reference efficiency	25	°C
Packing factor	0.8	

3.3. Heat Pump Model

A low-temperature water source heat pump (LHP) is applied in the heating mode and a high-temperature water source heat pump (HHP) is used as auxiliary device in the cooling mode. This combination mode is determined according to the previous experimental construction. Besides, the electrical energy produced by the LCPV/T system is used for driving heat pumps and circulating pumps.

3.3.1. Low Temperature Water to Water Heat Pump

The requirement of heat load is not satisfied by a single LCPV/T system when the temperature of storage tank 1 is between 15–40 °C. In this case, the LHP is turned on and the heat source comes from storage tank 1. Under the closed-loop condition, the performance of LHP is significantly improved.

Meanwhile, the inlet temperature of LCPV/T system decreases and the comprehensive efficiency is enhanced. When the temperature of storage tank 1 is below 15 °C, LHP is switched off because of the low energy efficiency. At this time, auxiliary natural gas heater directly provides hot water for space heating. The detail parameters of LHP are shown in Table 4.

Table 4. Description of the low-temperature water source heat pump (LHP).

Parameter	Value	Unit
Specific heat capacity of load side fluid	4190	J/(kg·°C)
Specific heat capacity of source side fluid	4190	J/(kg·°C)
Rated heating capacity	30,240	kJ/h
Rated coefficient of performance (COP)	3.8	-
Rated flow rate of condenser	2500	kg/h
Rated flow rate of evaporator	1200	kg/h
Rated heating temperature	48	°C
Rated inlet temperature of evaporator inlet temperature	15	°C

3.3.2. High Temperature Water to Water Heat Pump

The high temperature water source heat pump (HHP) is used to provide 85 °C–90 °C hot water as the heat source for the lithium bromide absorption chiller. The detailed parameters of HHP are shown in Table 5.

Table 5. Description of the high temperature water source heat pump (HHP).

Parameter	Value	Unit
Specific heat capacity of load side fluid	4190	J/(kg·°C)
Specific heat capacity of source side fluid	4190	J/(kg·°C)
Rated heating capacity	64,800	kJ/h
Rated coefficient of performance (COP)	2.5	-
Rated flow rate of condenser	4500	kg/h
Rated flow rate of evaporator	2500	kg/h
Rated heating temperature	90	°C
Rated inlet temperature of evaporator inlet temperature	30	°C

3.4. Lithium Bromide Absorption Chiller

For space cooling, a single-effect lithium bromide absorption chiller is employed during summer. The reason for choosing the absorption chiller is that it can effectively utilize the thermal energy generated by the LCPV/T system and improve the comprehensive utilization rate of the NG-LCPV/T-TG system. The parameters of the chiller are demonstrated in Table 6.

Table 6. Description of the lithium bromide absorption chiller.

Parameter	Value	Unit
Rated capacity	10	kW
Rated COP	0.6	-
Auxiliary electrical power	0.5	kW

3.5. Cooling Tower

The function of cooling tower is to cool down the steam in condenser into water. The cooling tower uses cold water as a circulating coolant. Meanwhile, the absorbed heat is discharged to the atmosphere with steam. The parameters of the cooling tower are demonstrated in Table 7.

Table 7. Description of the cooling tower.

Parameter	Value	Unit
Maximum cell flow rate	3000	m^3/h
Fan power at maximum flow	250	W
Natural convection cell flow rate	100	m^3/h
Sump volume	1.0	m^3
Initial sump temperature	15.0	°C
Mass transfer constant	1.36	
Mass transfer exponent	−0.94	

3.6. Natural Gas Auxiliary Heater

The output performance of the LCPV/T system is not stable due to the instability of solar energy. Additionally, natural gas is a traditional fossil energy with low pollution, low emission and high calorific value. The coupling of the two sorts of energy could reduce the irreversible loss of natural gas and enhance the utilization efficiency of solar energy. Therefore, the auxiliary natural gas heater is adopted in the proposed system to ensure the efficient and stable operation throughout one year. The auxiliary natural gas heater 1 is set under the heating mode, while the auxiliary natural gas heater 2 is set under the cooling mode. Detailed parameters of the auxiliary natural gas heater are manifested in Table 8.

Table 8. Description of the auxiliary natural gas heater.

Name	Parameter	Value	Unit
Auxiliary natural gas heater 1	Maximum heating rate	8.4	kW
	Specific heat of fluid	4190	J/(kg·°C)
	Overall loss coefficient for heater during operation	0.0	J/(kg·°C)
	Efficiency of auxiliary heater	1.0	-
Auxiliary natural gas heater 2	Maximum heating rate	18	kW
	Specific heat of fluid	4190	J/(kg·°C)
	Overall loss coefficient for heater during operation	0.0	J/(kg·°C)
	Efficiency of auxiliary heater	1.0	-

3.7. Pumps

The system consists of 5 circulating pumps, which make up the cycle of the NG-LCPV/T-TG system. The function of pump 1 is to import water from LCPV/T system into storage tank 1. Pump 2 is used to support the heating cycle of the experimental room. The function of pump 3 is to realize the cycle of hot water which can drive the absorption chiller. The pump 4 is used to support the cycle of cooling tower. Pump 5 is applied to realize the coolant cycle of the experimental room. The specific parameters of the circulating pumps are listed in Appendix A-Table A1.

3.8. Water Storage Tanks

Two storage tanks are installed in the proposed system. Storage tank 1 is utilized as the heat source of the NG-LCPV/T-TG system. It stores the hot water heated by LCPV/T system. Storage tank 2 works as the inlet water tank of the LCPV/T system. The basic parameters of the tanks are demonstrated in Appendix A-Table A2.

4. Results and Discussion

Since this research is to investigate the full-condition performance of the NG-LCPV/T-TG system, the data of continuous operation in one year is simulated. The experimental data in reference [26] is

used for the verification of the model used in this article. Take the COP value of the lithium bromide absorption chiller, as a parameter for comparison. The average deviation value of the modeling results with the experimental results is 10%, and the maximum value is 18%. These errors are mainly caused due to the start and stop of the equipment in the experiment, which causes the COP value to be lower than the simulated value. However, an acceptable range is observed among the results. Therefore, the models presented in this paper are feasible and reliable to simulate the performance of the trigeneration system.

The location simulated by the proposed system is Beijing, China. Beijing is a city with four distinct seasons throughout the year. Outdoor meteorological parameters mainly focus on solar radiation intensity, wind speed and outdoor ambient temperature. The annual variation of these three parameters are manifested in Figure 4. This meteorological parameter uses the CN-Beijing-545110.tm2 from Meteonorm in TRNSYS software. Both load of the experimental room and LCPV/T performance are affected by outdoor meteorological parameters.

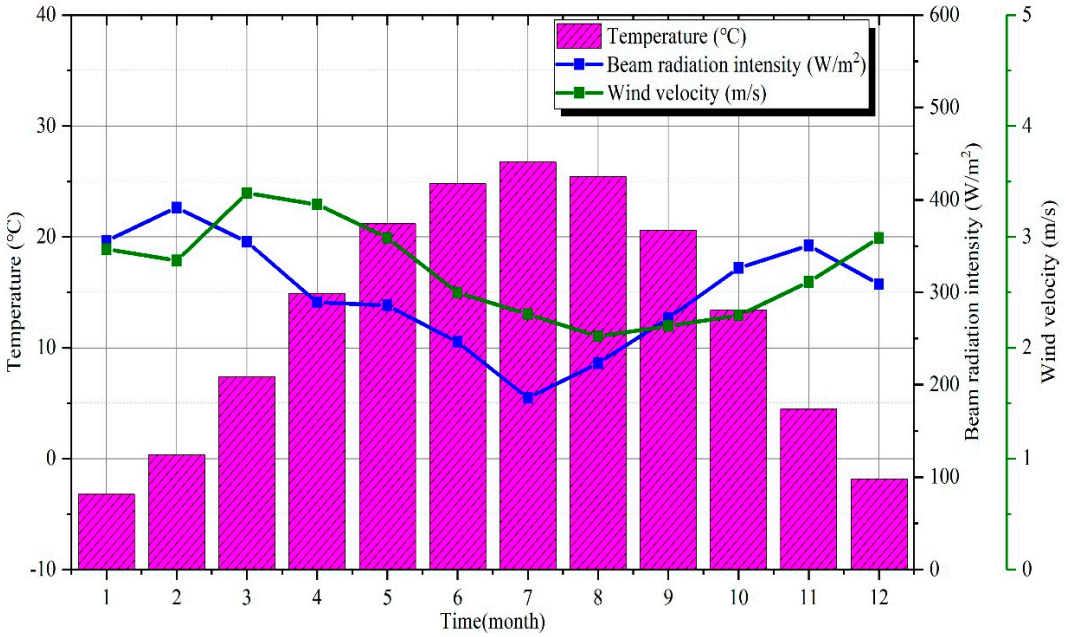

Figure 4. The curve of meteorological parameters throughout one year.

Moreover, the average beam radiation intensity of Beijing in summer is lower than that in winter. This is because Beijing is frequently rainy in summer. The daul-axis tracking system is applied such that the beam radiation is always normal to the surface of PV cells. Because the low-concentrating technology is adopted, only beam radiation intensity has an impact on the performance of the proposed system. In Figure 4, the average value of beam radiation intensity per month is calculated according to the sum of hours that has solar radiation each day. The maximum and minimum amount of the average beam radiation intensity are 391.8 W/m^2 in February and 185.7 W/m^2 in July. In addition, the hours for calculating average value of ambient temperature and wind velocity are the sum of hours in a whole day per month. The detailed number of hours used for calculating the average value per month are listed in Appendix A-Table A3. The ambient temperature follows a seasonal law such that is high in summer and low in winter. In winter, it is maintained at around 0 °C. The height measurement for wind velocity is 10 m. The wind speed is slightly higher in March and April.

In order to maintain comfortable, the temperature of the experimental room is controlled around 20 °C during winter and around 25 °C during summer. The allowable fluctuation range is 1 °C. A reference room that is not provided space heating and cooling is set for comparison. As demonstrated in Figure 5, the temperature of the reference room is associated with the outdoor ambient temperature.

In contrast, the temperature of the experimental room is comfortable throughout the year due to the effect of the NG-LCPV/T-TG system.

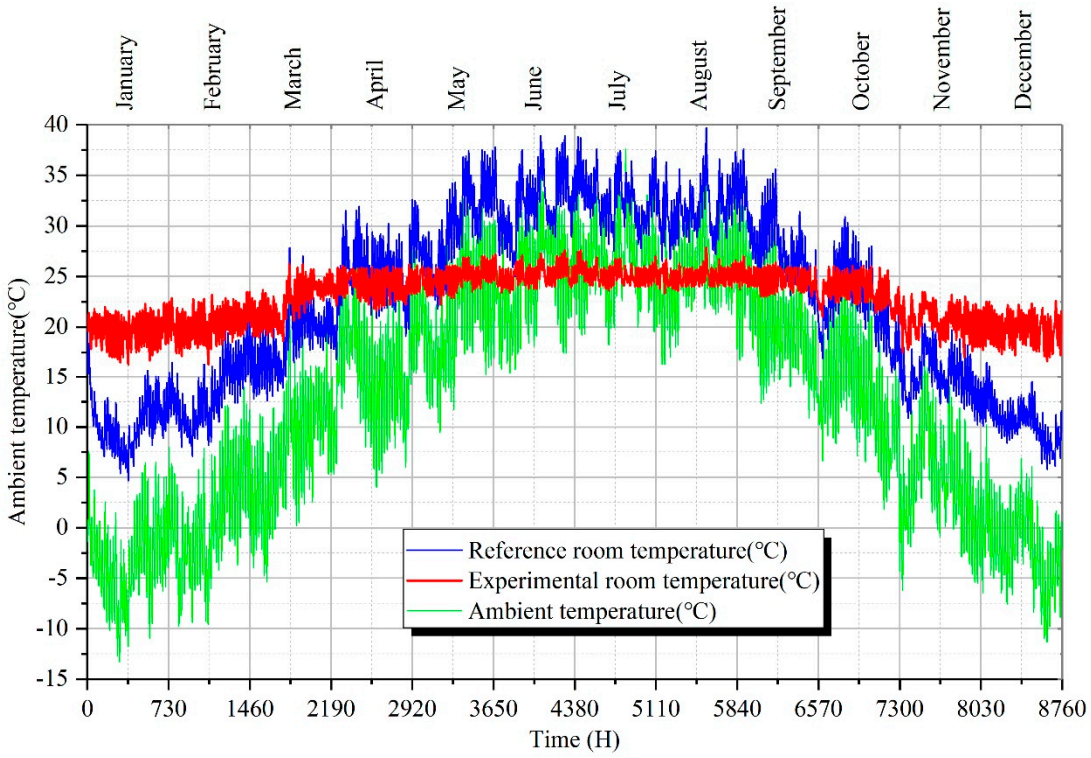

Figure 5. The temperatures of experimental, reference room, and ambient throughout one year.

Figure 6 depicts variations of the electrical and thermal energy produced by the LCPV/T system during a day. In this paper, the 240th hour to 264th hour (24 h) is randomly selected as a typical day. The maximum amount of the electrical and thermal energy are 2.4 kW and 11.1 kW, respectively. The cumulative value of the electrical energy is 16.4 kWh, and the cumulative thermal energy is 73.5 kWh. In summary, the LCPV/T system has excellent capacity for producing electrical and thermal energy simultaneously.

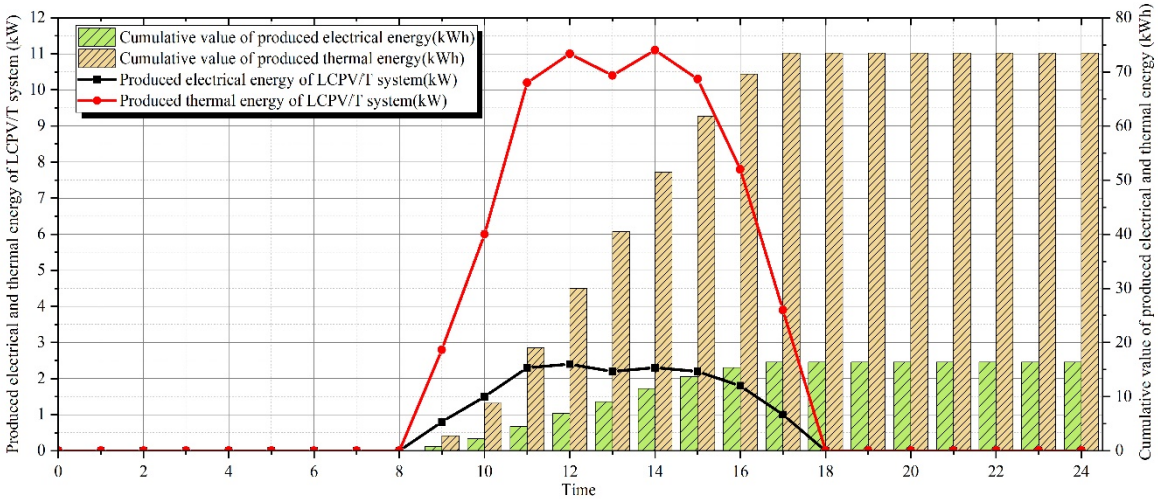

Figure 6. Produced electrical and thermal energy of LCPV/T system during a day (240 h~264 h).

As shown in Figures 7 and 8, the electrical and thermal energy produced by the LCPV/T system during one year is presented. At the 7883th hour, when the radiation intensity is 776 W/m^2,

the maximum amount of electrical energy is 2.53 kW. At the 7885th hour, when the radiation intensity is 805 W/m^2, the maximum amount of thermal energy is 13.85 kW. The electrical energy and thermal energy are affected by the radiation intensity.

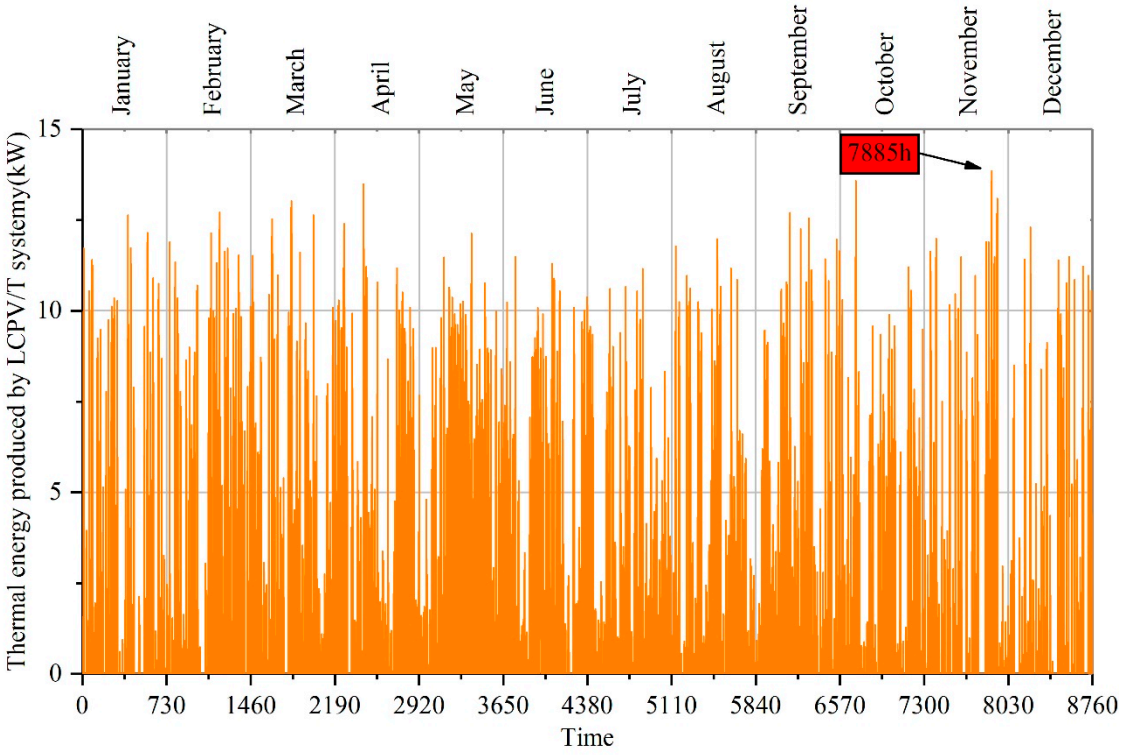

Figure 7. Produced thermal energy of LCPV/T system during a year.

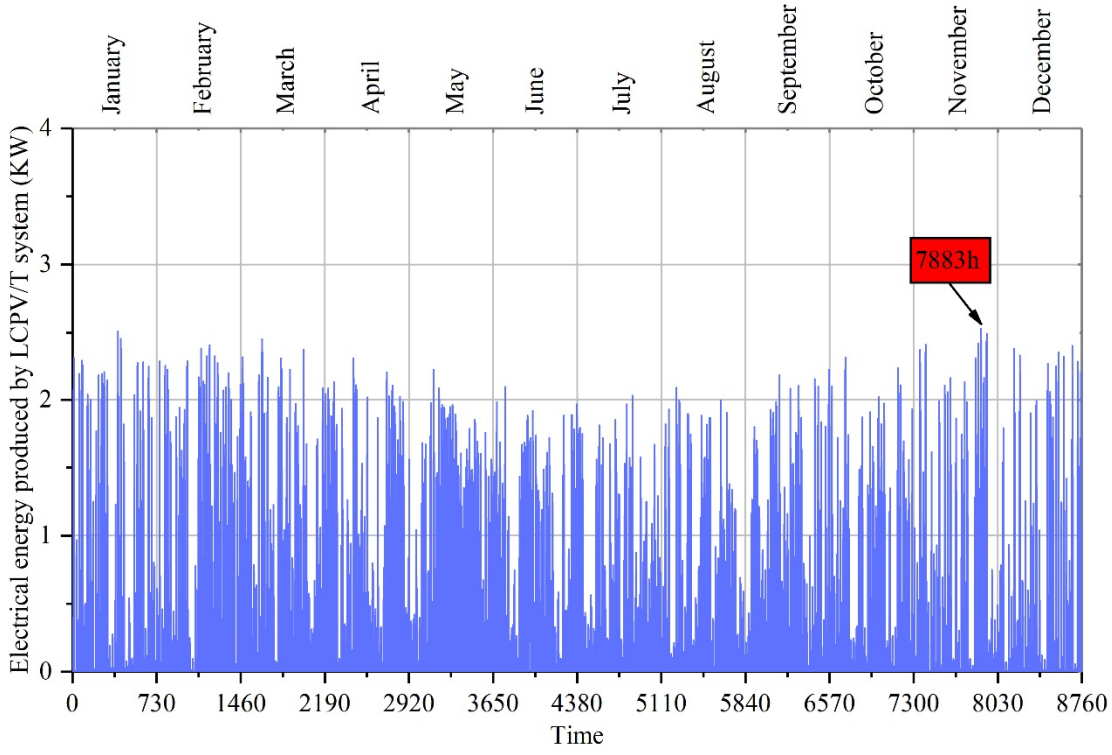

Figure 8. Produced electrical energy of LCPV/T system during a year.

The outlet water temperature on a day and a year of the LCPV/T system are obviously obtained in Figures 9 and 10, respectively. The supreme outlet temperature in a day is detected at nearly 45 °C. In addition, the outlet temperature gradually rises from 08:00 and increases rapidly at 10:00, then decreases until 16:00. The outlet temperature in one year is around 45 °C, which only reaches 65 °C for a few days in summer. The lowest temperature in winter is relatively low, while that in summer is about 20 °C.

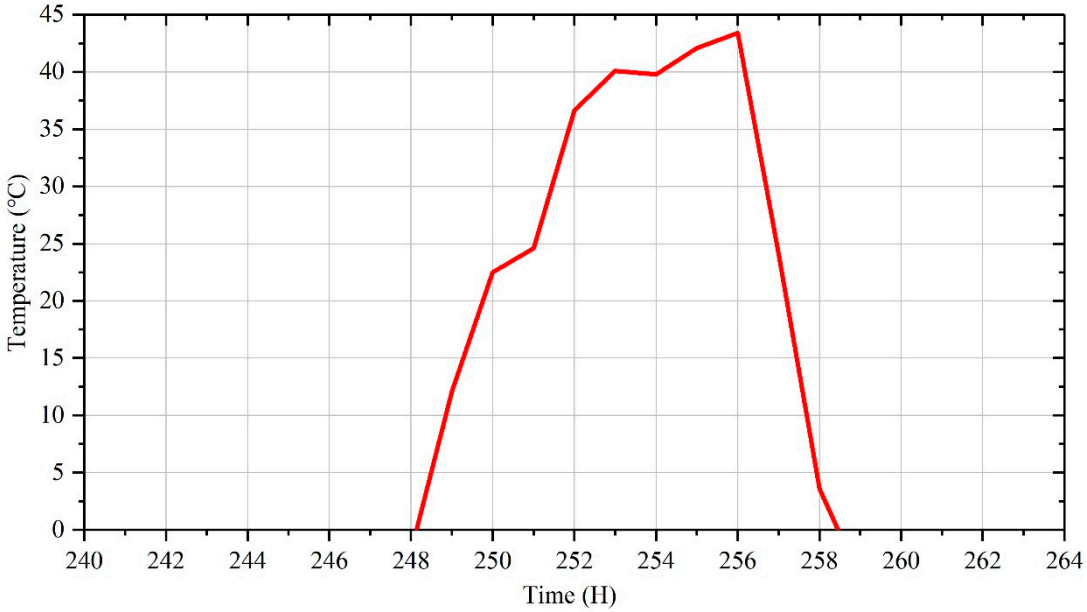

Figure 9. Outlet temperature changes of the LCPV/T model on one day (240 h~264 h).

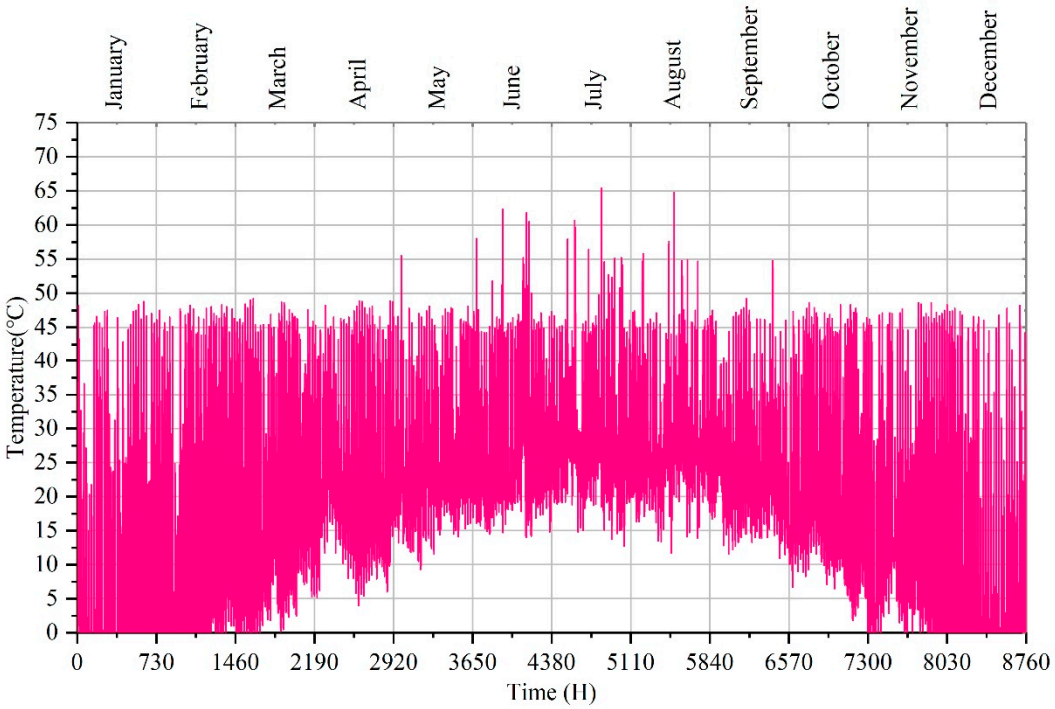

Figure 10. Outlet temperature changes of the LCPV/T model during a year.

In particular, the temperature of the storage tank is not below zero in the non-operation stage of LCPV/T system (shown in Figure 11) due to the heat storage property. Because of the thermal inertia, the rising time of water temperature in the storage tank is later than that the rising time of the outlet

temperature of the LCPV/T system. Moreover, the temperature of storage tank 1 after 18:00 exceeds that before 08:00. As shown in Figure 12, the temperature of tank 1 is maintained between 10–45 °C throughout the year. Consequently, storage tank 1 can be treated as a stable cryogenic heat source of the NG-LCPV/T-TG system.

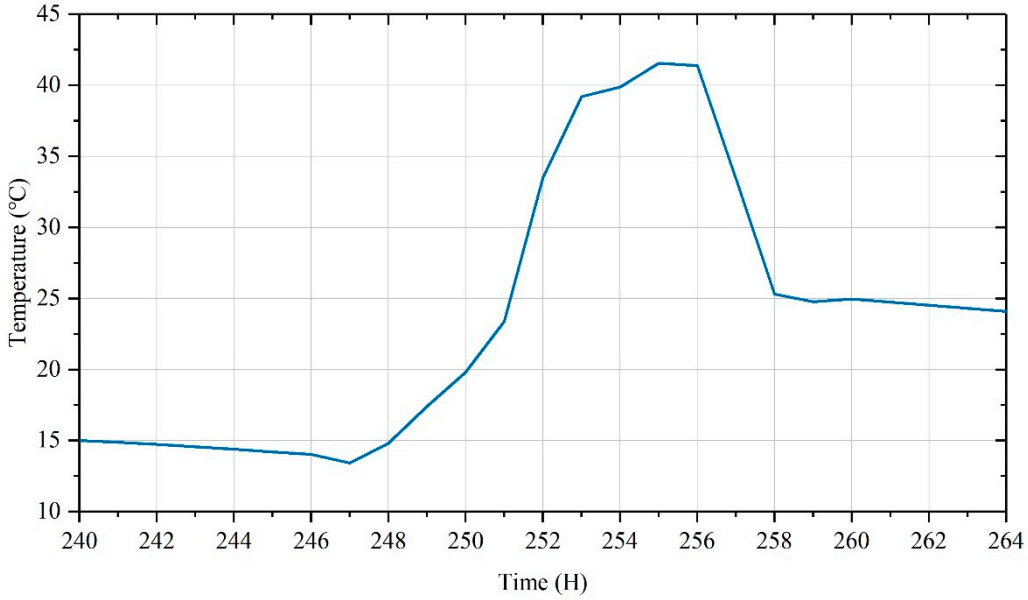

Figure 11. Temperature of storage tank 1 on a day (240 h~264 h).

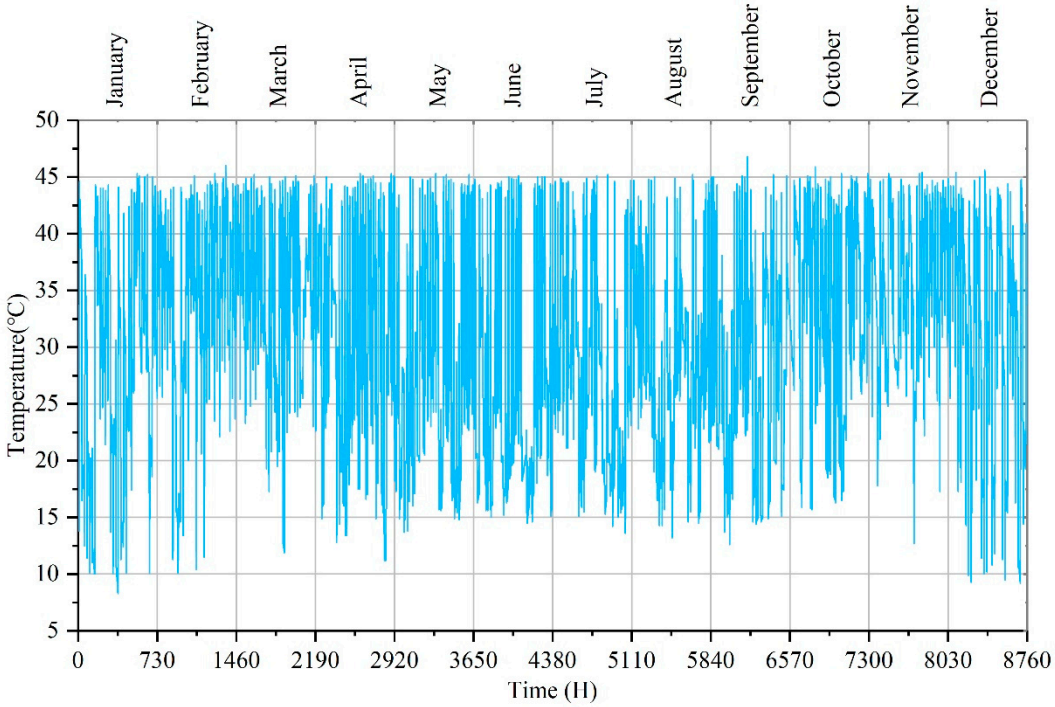

Figure 12. Temperature of storage tank 1 for one year.

In the heating mode, it is clearly visible that the LHP is on when the temperature of storage tank 1 is between 15 °C and 40 °C. Additionally, when the temperature of storage tank 1 is below 15 °C, the auxiliary natural gas heater is applied. As shown in Figure 13, the time nodes of heating mode are the 1761th hour and 7328th hour, respectively. Additionally, the COP of the LHP is around 5, which indicates a significant improvement compared with the rated value of 3.8. Since the terminal of

heat dissipation adopts capillary network system, the outlet water temperature at the load side of the LHP is maintained at about 35 °C to satisfy the temperature requirements of the experimental room. Obviously, such a combination takes sufficient advantage of the low temperature heat source, and makes a remarkable contribution to saving energy.

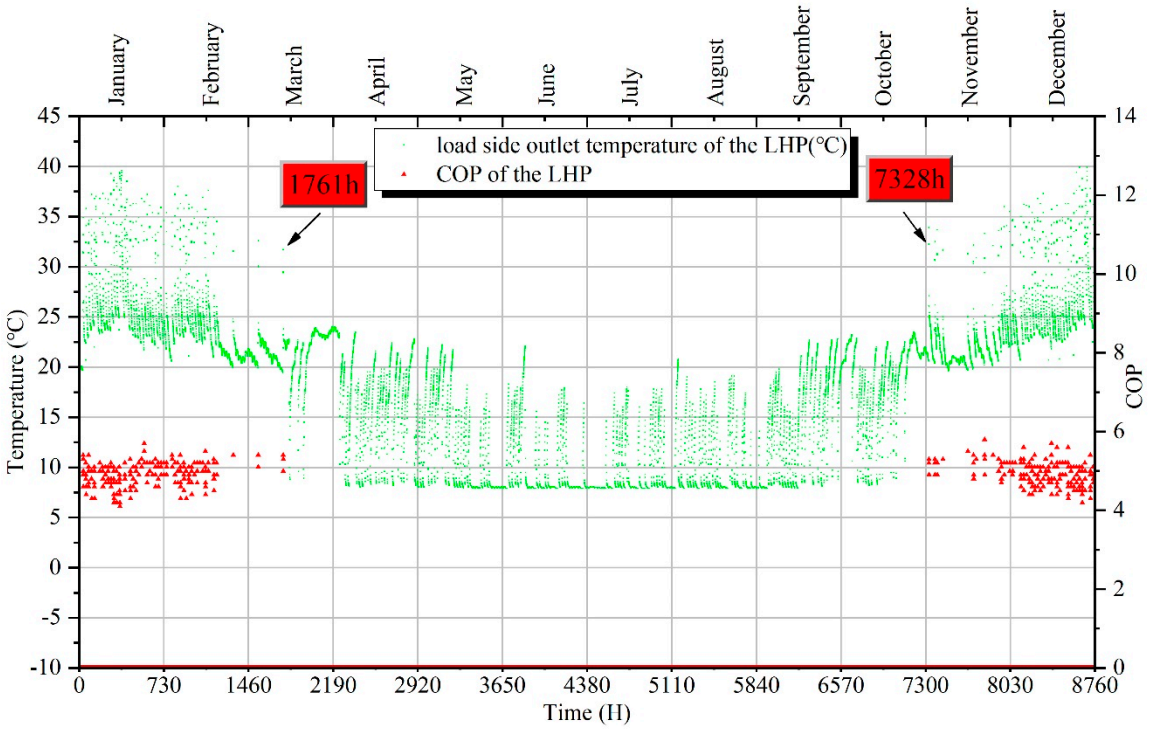

Figure 13. Coefficient of performance (COP) and load side outlet temperature of the LHP during a year.

Figure 14 clearly shows the proportion of the thermal energy produced by LHP and NGAH in heating mode, respectively. When the thermal energy exceeds the demand of space heating, it will preheat domestic hot water. Obviously, the produced thermal energy is higher than the heat load of the experimental room. Furthermore, the produced thermal energy of NGAH is higher than that of the LHP in January and December. The reason for this is that the outdoor environment temperature is low, and the radiation intensity is weak in January and December. Under the above environment conditions, the thermal energy produced by LCPV/T system is slighter, which leads to the low temperature of storage tank 1. In February and November, the produced thermal energy of the LHP is significantly higher than that of the NGAH, because the outdoor environment temperature and the radiation intensity increase significantly in February and November.

In addition, the monthly data relevant to the accumulated thermal energy under the heating mode is listed in Table 9. In January, the heat load is the highest, with the accumulated value up to 906 kWh. The thermal energy produced by the LHP and the NGAH are 311 kWh and 664 kWh, respectively. Besides, the thermal energy to preheat domestic hot water is 573 kWh. In particular, the maximum amount of preheating domestic hot water is 928 kWh in February. Furthermore, LCPV/T system provides 131 kWh thermal energy for heating directly. The thermal energy produced by NGAH is only 101 kWh and 17 kWh in February and November.

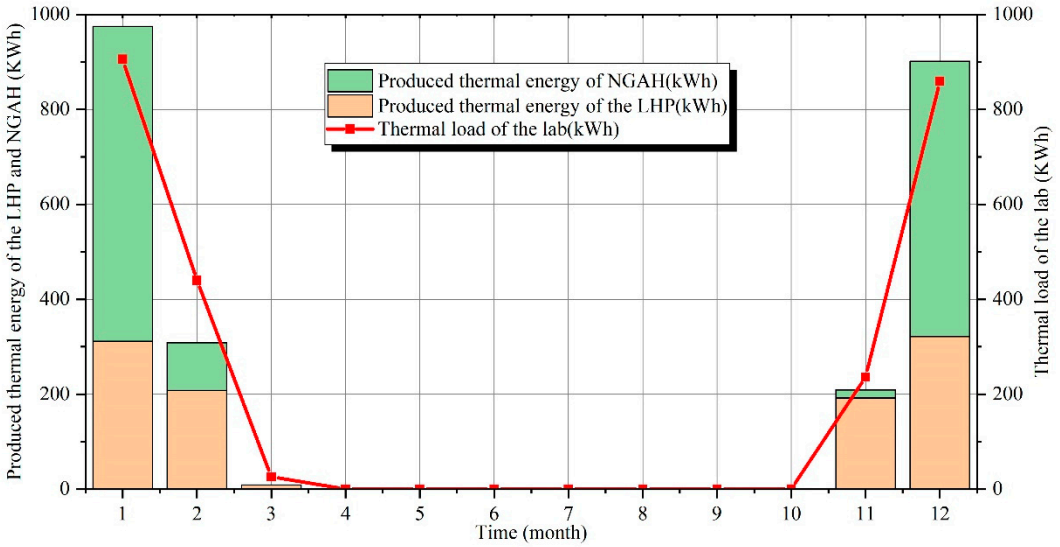

Figure 14. Produced thermal energy of natural gas auxiliary heater (NGAH) and LHP during heating mode.

Table 9. Produced thermal energy in heating mode.

Month	Thermal Load (kWh)	LHP (kWh)	NGAH (kWh)	Domestic Hot Water (kWh)
January	906	311	664	573
February	440	208	101	928
November	236	192	17	793
December	860	322	580	286

In cooling mode, the HHP provides 85–90 °C hot water as the heat source of the chiller. Figure 15 refers to the performance when outlet temperature of HHP maintained at about 90 °C in a stable manner. In addition, the COP of HHP can reach 2.2. Because the outlet temperature on the load side of HHP is high, the COP is lower than that of LHP.

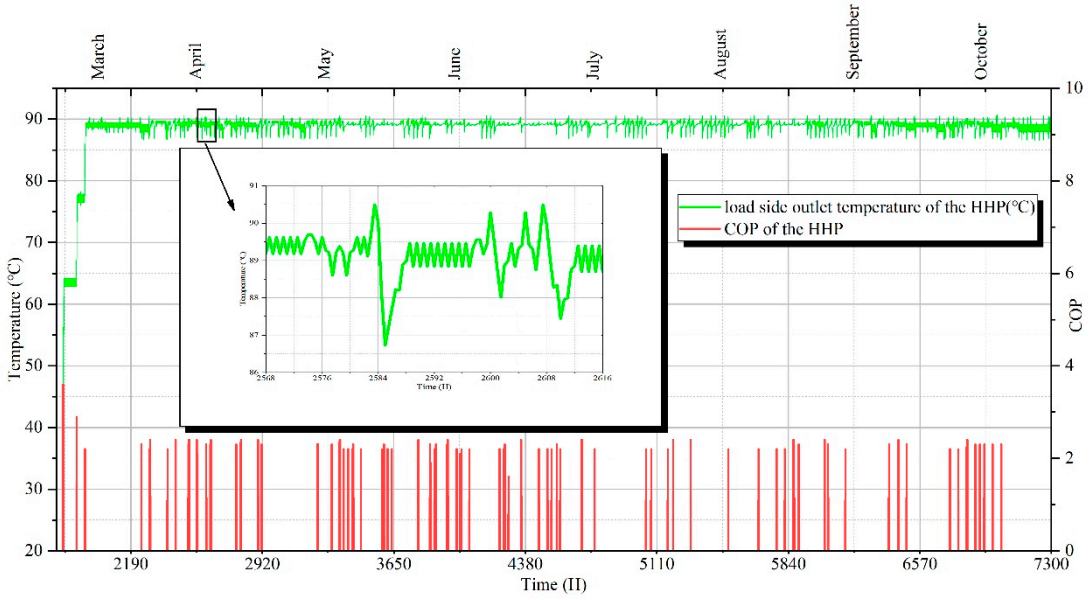

Figure 15. COP and load side outlet temperature of the HHP during cooling mode.

Figure 16 depicts that the single-effect absorption chiller can run continuously with the COP up to 0.7 in a year. The COP for this model is defined as the energy transferred from the chilled water divided by the sum of the electrical energy required by the chiller and the energy provided to the chiller by the inlet hot water. Since the energy consumed by an absorption chiller is mainly the heat energy, energy efficiency ratio (EER) is often used as the economic evaluation index. The EER is the ratio of the cooling capacity obtained by the absorption chiller to the heat consumed. The maximum amount of the EER is 0.69 during a year. The chiller is closed when the experimental room falls below 26 °C. Moreover, in the cooling mode, the capillary network system is adopted as well. The outlet temperature of the chiller is generally maintained between 10–20 °C, which can fulfil the requirement of space cooling.

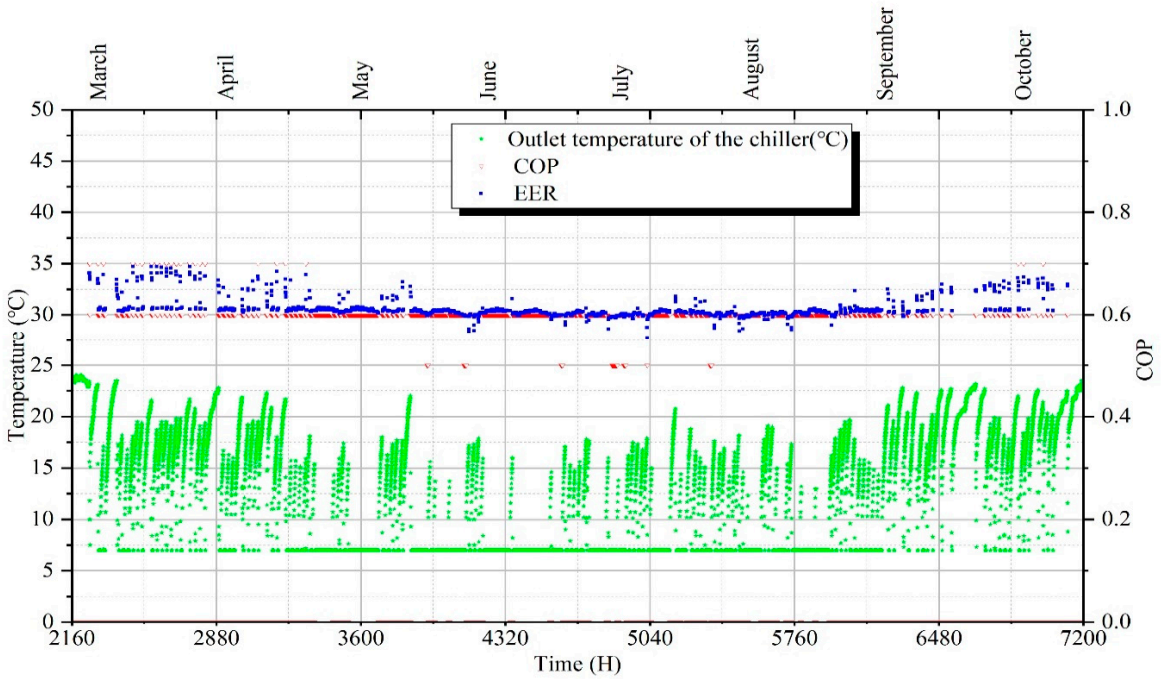

Figure 16. COP, energy efficiency ratio (EER) and outlet temperature of the chiller during cooling mode.

Figure 17 demonstrates the outlet temperature curve of the cooling tower. The cooling tower is started only when the chiller is running. Obviously, the outlet temperature of the cooling tower is higher when the demand of the cooling load is large. Cooling tower outlet water temperature is up to 30 °C, which can fulfill the demand of the chiller.

Table 10 lists the cooling capacity and thermal energy produced in the cooling mode. In March, the cooling load is relatively low, so the energy demand is small. At the same time, the radiation intensity increases compared with that in winter. Therefore, the thermal energy to preheat domestic hot water is the highest in March, up to 1295 kWh. As the ambient temperature rises gradually, the cooling load increases, then the cooling capacity needed is increased. It is also worth noting that the maximum amount of cooling load is 1655 kWh in July. The cooling capacity provided by the chiller is 2389 kWh. The auxiliary natural gas heater is the main heat source of the chiller which provided 3297 kWh thermal energy. In addition, the minimum preheated thermal energy of domestic hot water is 104 kWh in July.

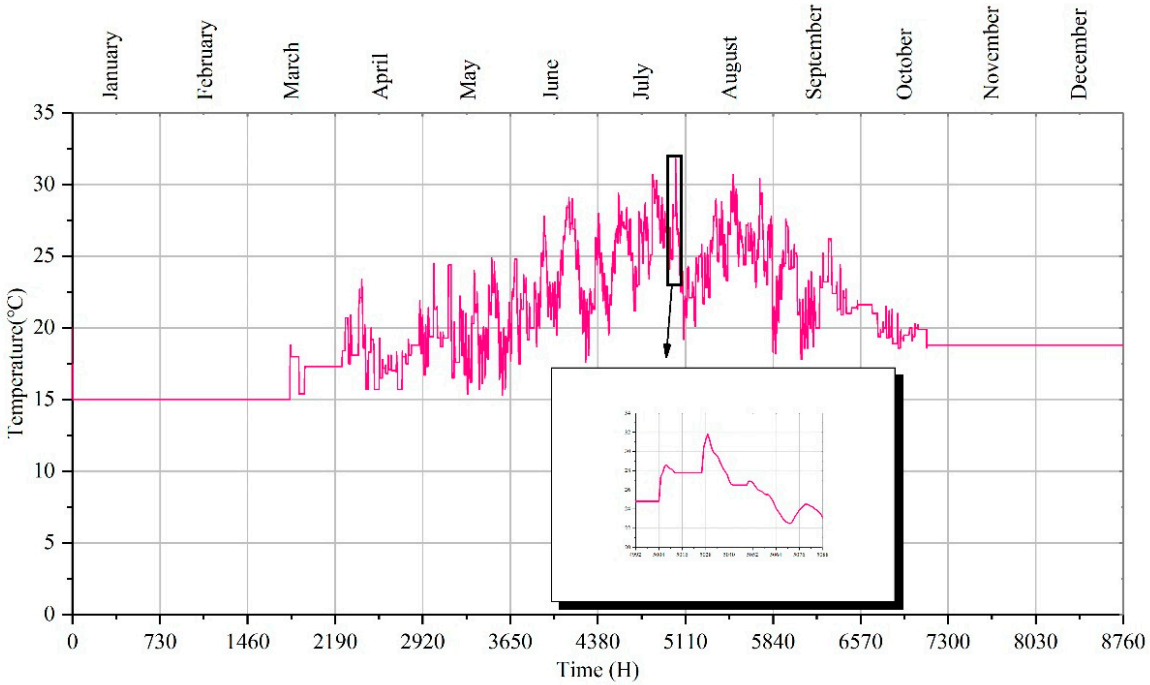

Figure 17. The outlet temperature of cooling tower during a year.

Table 10. Produced energy in cooling mode.

Month	Cooling Load (kWh)	Chiller (kWh)	HHP (kWh)	NGAC (kWh)	Domestic Hot Water (kWh)
March	16	135	67	180	1295
April	430	1014	135	1254	775
May	1035	1956	168	2573	400
June	1351	2218	80	1356	121
July	1655	2389	75	3297	104
August	1490	2216	73	2822	184
September	803	1545	96	2108	427
October	223	356	55	887	766

Figure 18 clearly draws the cooling load and the cooling capacity provided by the chiller under the cooling mode. The cooling capacity of the chiller is greater than the cooling load of the room. Due to the fluctuation of the indoor temperature and thermal loss of the water tanks, the cooling capacity provided by the chiller is greater than the cooling load. It is also apparent from Figure 18 that most of the thermal energy required during summer is supplied by the NGAC. This is because the temperature of storage tank 1 is set at 40 °C when the system determines the mode of heat source supply. In Beijing, although the ambient temperature is high, the radiation intensity is not high enough in summer. Thus, the thermal energy produced by the LCPV/T system cannot satisfy the temperature requirement of the chiller. At this time, the heat source of the chiller is mostly supported by the natural gas heater, which has more economic and energy saving benefits.

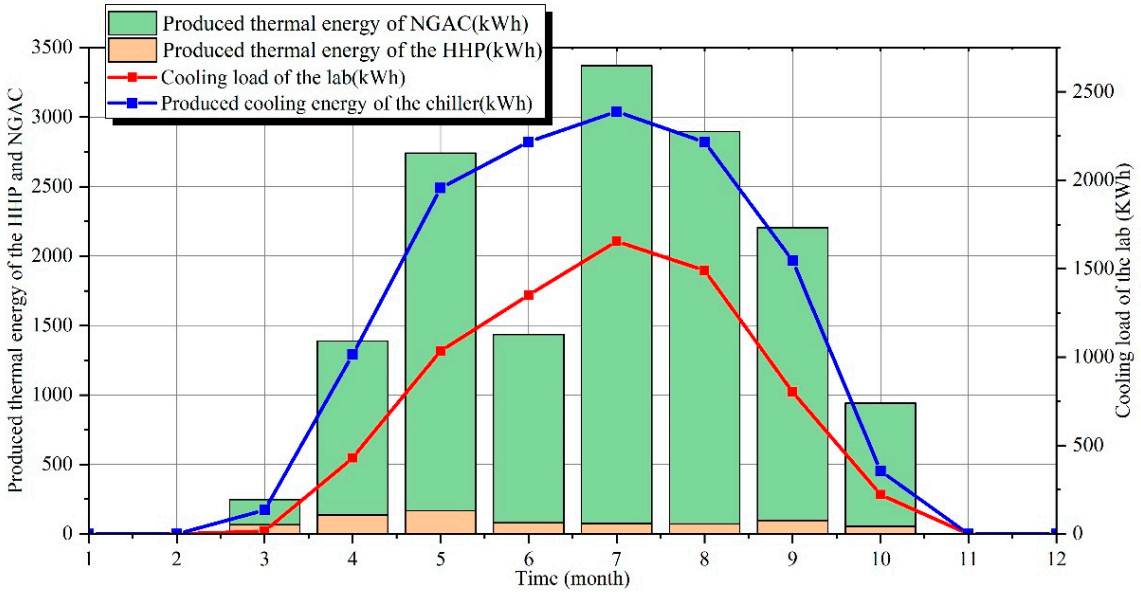

Figure 18. Produced thermal energy of NGAC and HHP during cooling mode.

Conspicuously, Figure 19 demonstrates the power consumption of all the electrical equipment of the proposed system and produced electrical energy of LCPV/T system in one year. In the heating mode, electrical energy produced by the LCPV/T system is sufficient to meet the power consumption of the LHP and circulating water pumps (pump 1 and pump 2) in the proposed system. Nevertheless, the electrical energy produced by the LCPV/T system can only satisfy the power consumption of the chiller and the HHP in the cooling mode. The power consumption of the circulating water pumps (pump 3, pump 4, and pump 5) are supported by external grid power. In addition, since the selection of the three pumps is based on the data of previous experiment, the energy consumption of the pumps is too large. Future research will further optimize the energy consumption of the pumps.

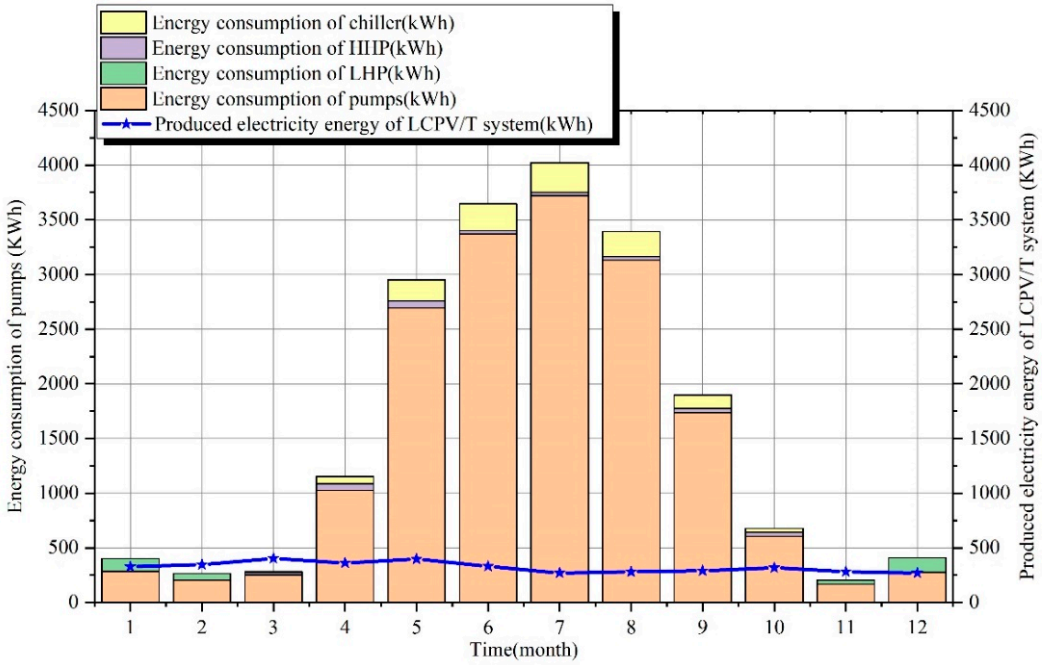

Figure 19. Energy consumption of NG-LCPV/T-TG system.

In particular, the specific data of the power consumption and electrical energy produced by the LCPV/T system are listed in Table 11. According to the data, the maximum amount of the electrical energy produced by LCPV/T is 403.6 kWh in April. In July, the maximum power consumption of the circulating pumps, chiller and HHP are 3370.5 kWh, 245.5 kWh, and 30.3 kWh, respectively. The maximum amount of the power consumption of HHP is 64.9 kWh in May. In February, March and November, the power consumption and the electrical energy produced by the LCPV/T system are balanced. Nevertheless, some power needs to be purchased from the grid in other months. The proposed system can simultaneously provide the space cooling and heating, part of the electrical energy required in the building, throughout the year.

Table 11. Power consumption and produced of NG-LCPV/T-TG system equipment for one year.

Month	Produced Electricity by LCPV/T (kWh)	Chiller (kWh)	HHP (kWh)	LHP (kWh)	Pumps (kWh)
January	328.4	0	0	116.5	286.5
February	346.3	0	0	61.2	204.5
March	403.6	7	20.8	1.8	253.5
April	361.6	66	60	0	1026
May	397.6	192.5	64.9	0	2693.5
June	332.3	245.5	30.3	0	3370.5
July	269.8	272.5	29.2	0	3721.5
August	280.5	228	31	0	3133
September	290.9	122	37.6	0	1737
October	317.8	36	37.2	0	605.5
November	282.1	0	0	36.1	168.5
December	269.5	0	0	134.2	275

5. Conclusions

In the present paper, a design and transient analysis of an NG-LCPV/T-TG system is demonstrated. The continuous operation of the proposed system is realized by TRNSYS software throughout the year. In addition, the building model is set up according to the real data of the experimental room in our previous work. The main component of this system is the LCPV/T system, which adopts the low-concentrating technology to provide electrical energy and low-temperature thermal energy at the same time. The auxiliary equipment of heating mode adopts LHP and a natural gas heater. In the cooling mode, the single-effect absorption lithium bromide absorption chiller is applied. Moreover, the HHP and the natural gas auxiliary heater are used as auxiliary heat source for the chiller. In addition, the coupling method of traditional energy natural gas and renewable energy solar energy is proposed. Based on previous work, this research obtains the operation data of various equipment throughout the year, which proved the feasibility of the trigeneration system. The main outcomes of this paper are as follows:

- The proposed system maintains the experimental room at 25 °C under the cooling mode and 20 °C under the heating mode.
- The maximum amount of the electrical and thermal energy during a day are 2.4 kW and 11.1 kW, respectively. Moreover, 16.4 kWh of electrical energy and 73.5 kWh of thermal energy are produced by the LCPV/T system for a day. In addition, the maximum amount of electrical and thermal energy are 2.53 kW and 13.85 kW in a year. The electrical and thermal energy produced by the LCPV/T system throughout the year are 3819 kWh and 18,374 kWh.

- During the heating mode, the COP of LHP reaches 5. The outlet water temperature at the load side of the LHP is about 35 °C. The produced thermal energy of the LHP and the NGAH are 311 kWh and 664 kWh in January. In particular, the highest thermal energy for preheating domestic hot water is 928 kWh in February. LCPV/T system provides 131 kWh thermal energy for heating directly. The thermal energy produced by NGAH is only 101 kWh and 17 kWh in February and November.
- In the cooling mode, the average COP of HHP is 2.2. The maximum COP and EER of the single-effect absorption chiller are 0.7 and 0.9, respectively. It is also worth noting that the maximum amount of cooling load is 1655 kWh in July. The cooling capacity provided by the chiller is 2389 kWh. The auxiliary natural gas heater is the main heat source of the chiller which provided 3297 kWh thermal energy.
- In this research, the maximum amount of the electrical energy produced by LCPV/T system is 403.6 kWh in April. In July, the maximum power consumption of the circulating pumps, chiller and HHP are 3370.5 kWh, 245.5 kWh, and 30.3 kWh, respectively. The maximum power consumption of HHP is 64.9 kWh in May.

In summary, the proposed system can simultaneously produce electricity, undertake space cooling and heating and produce domestic hot water. It can improve the conversion efficiency of the LCPV/T system, improve the thermal economy of a natural gas thermal system, reduce pollutant emissions, and reduce the irreversible loss of natural gas combustion. Our future work will be to discuss the optimization design of the NG-LCPV/T-TG system.

Author Contributions: Y.L. developed the overall dynamic simulation model. H.Y. and N.W. were mainly engaged in chart drawing. H.Z. and H.C. provided the overall idea of the article. All authors have read and agreed to the published version of the manuscript.

Funding: This work was supported by Key Research and Development Program of Hebei Province (18214318D), Beijing Municipal Science and Technology Project (Z151100003515002) and China Postdoctoral Science Foundation (2019M660595).

Conflicts of Interest: The authors declare that they have no known competing financial interests or personal relationships that could have appeared to influence the work reported in this paper.

Nomenclature

COP	Coefficient of performance
CPC	Compound parabolic concentrator
CPV/T	Concentrating photovoltaic /thermal
EER	Energy efficiency ratio
HHP	High-temperature water source heat pump
LCPV/T	Low-concentrating photovoltaic /thermal
LHP	Low-temperature water source heat pump
NGAC	Natural gas assisted cooling mode
NGAH	Natural gas assisted heating mode
NG-LCPV/T-TG	Natural gas assisted solar low-concentrating photovoltaic/thermal trigeneration system
PV/T	Photovoltaic/thermal

Appendix A

Table A1. Depiction of circulation pumps in the NG-LCPV/T-TG system.

Serial Number	Name	Parameter	Value	Unit
Pump 1	Source side pump	Rated flow rate Fluid specific heat Rated power	1200 4190 0.5	kg/h J/(kg·°C) kW
Pump 2	Heating pump	Rated flow rate Fluid specific heat Rated power	3000 4190 0.5	kg/h J/(kg·°C) kW
Pump 3	High temperature circulating pump	Rated flow rate Fluid specific heat Rated power	4500 4190 4.5	kg/h J/(kg·°C) kW
Pump 4	Cooling pump	Rated flow rate Fluid specific heat Rated power	6000 4190 1.5	kg/h J/(kg·°C) kW
Pump 5	Refrigerant pump	Rated flow rate Fluid specific heat Rated power	3000 4190 0.5	kg/h J/(kg·°C) kW

Table A2. Depiction of the water storage tanks.

Parameter	Value	Unit
Tank volume	0.3	m^3
Fluid specific heat	4190	J/(kg·°C)
Fluid density	1000.0	kg/m^3
Tank loss coefficient	0.4	$W/(m^2 \cdot °C)$
Height of node	0.1	m
Set point temperature	60	°C
Deadband for heating	5.0	Δ°C
Maximum heating rate	9000	kJ/h
Boiling point	100	°C

Table A3. Detailed amount of hours for calculating average value per month.

Parameters \ Month(h)	1	2	3	4	5	6	7	8	9	10	11	12
Beam radiation intensity	260	249	321	336	382	358	357	336	302	275	228	239
Ambient temperature	744	672	744	720	744	720	744	744	720	744	720	744
Wind velocity	744	672	744	720	744	720	744	744	720	744	720	744

References

1. BP. Statistical Review of World Energy. 2020. Available online: https://www.bp.com/en/global/corporate/energy-economics/statistical-review-of-world-energy.html (accessed on 13 August 2020).
2. Research and Analysis of Electric Power Development in the Period of 14th Five-Year Plan. 2020. Available online: http://news.bjx.com.cn/html/20200619/1082527.shtml (accessed on 5 July 2020).
3. Jiang, K.; Du, X.; Kong, Y.; Xu, C.; Ju, X. A comprehensive review on solid particle receivers of concentrated solar power. *Renew. Sustain. Energy Rev.* **2019**, *116*, 109463. [CrossRef]
4. Aubé, F. Guide for Computing Carbon Dioxide Emissions Related to Energy Use. *Nat. Gas.* **2001**, *37*, 2–4.

5. Xu, C.; Bai, P.; Xin, T.; Hu, Y.; Xu, G.; Yang, Y. A novel solar energy integrated low-rank coal fired power generation using coal pre-drying and an absorption heat pump. *Appl. Energy* **2017**, *200*, 170–179. [CrossRef]
6. International Energy Agency (IEA). World Energy Investment 2019: Methodology Annex & Glossary of Key Terms. Available online: https://www.iea.org/reports/world-energy-investment-2019 (accessed on 16 December 2019).
7. Daneshazarian, R.; Cuce, E.; Cuce, P.M.; Sher, F. Concentrating photovoltaic thermal (CPVT) collectors and systems: Theory, performance assessment and applications. *Renew. Sustain. Energy Rev.* **2018**, *81*, 473–492. [CrossRef]
8. Settino, J.; Sant, T.; Micallef, C.; Farrugia, M.; Spiteri Staines, C.; Licari, J.; Micallef, A. Overview of solar technologies for electricity, heating and cooling production. *Renew. Sustain. Energy Rev.* **2018**, *90*, 892–909. [CrossRef]
9. Chen, H.; Zhang, H.; Li, M.; Liu, H.; Huang, J. Experimental investigation of a novel LCPV/T system with micro-channel heat pipe array. *Renew. Energy* **2018**, *115*, 773–782. [CrossRef]
10. Zhang, H.; Chen, H.; Han, Y.; Liu, H.; Li, M. Experimental and simulation studies on a novel compound parabolic concentrator. *Renew. Energy* **2017**, *113*, 784–794. [CrossRef]
11. Chow, T.T. A review on photovoltaic/thermal hybrid solar technology. *Appl. Energy* **2010**, *87*, 365–379. [CrossRef]
12. Zhang, H.; Chen, H.; Liu, H.; Huang, J.; Guo, X.; Li, M. Design and performance study of a low concentration photovoltaic-thermal module. *Int. J. Energy Res.* **2018**, *42*, 2199–2212. [CrossRef]
13. Li, G.; Pei, G.; Ji, J.; Yang, M.; Su, Y.; Xu, N. Numerical and experimental study on a PV/T system with static miniature solar concentrator. *Sol. Energy* **2015**, *120*, 565–574. [CrossRef]
14. Wang, Z.; Wei, J.; Zhang, G.; Xie, H.; Khalid, M. Design and performance study on a large-scale hybrid CPV/T system based on unsteady-state thermal model. *Sol. Energy* **2019**, *177*, 427–439. [CrossRef]
15. Widyolar, B.K.; Abdelhamid, M.; Jiang, L.; Winston, R.; Yablonovitch, E.; Scranton, G.; Cygan, D.; Abbasi, H.; Kozlov, A. Design, simulation and experimental characterization of a novel parabolic trough hybrid solar photovoltaic/thermal (PV/T) collector. *Renew. Energy* **2017**, *101*, 1379–1389. [CrossRef]
16. Ramos, A.; Chatzopoulou, M.A.; Guarracino, I.; Freeman, J.; Markides, C.N. Hybrid photovoltaic-thermal solar systems for combined heating, cooling and power provision in the urban environment. *Energy Convers. Manag.* **2017**, *150*, 838–850. [CrossRef]
17. Braun, R.; Haag, M.; Stave, J.; Abdelnour, N.; Eicker, U. System design and feasibility of trigeneration systems with hybrid photovoltaic-thermal (PVT) collectors for zero energy office buildings in different climates. *Sol. Energy* **2020**, *196*, 39–48. [CrossRef]
18. Su, B.; Han, W.; Qu, W.; Liu, C.; Jin, H. A new hybrid photovoltaic/thermal and liquid desiccant system for trigeneration application. *Appl. Energy* **2018**, *226*, 808–818. [CrossRef]
19. Huang, W.; Wang, J.; Xia, J.; Zhao, P.; Dai, Y. Performance analysis and optimization of a combined cooling and power system using low boiling point working fluid driven by engine waste heat. *Energy Convers. Manag.* **2019**, *180*, 962–976. [CrossRef]
20. Wang, J.; Xie, X.; Lu, Y.; Liu, B.; Li, X. Thermodynamic performance analysis and comparison of a combined cooling heating and power system integrated with two types of thermal energy storage. *Appl. Energy* **2018**, *219*, 114–122. [CrossRef]
21. Wang, J.; Yang, Y. A hybrid operating strategy of combined cooling, heating and power system for multiple demands considering domestic hot water preferentially: A case study. *Energy* **2017**, *122*, 444–457. [CrossRef]
22. Li, C.; Liu, J.; Zheng, S.; Chen, X.; Li, J.; Zeng, Z. Performance analysis of an improved power generation system utilizing the cold energy of LNG and solar energy. *Appl. Therm. Eng.* **2019**, *159*, 113937. [CrossRef]
23. Calise, F.; Dentice d'Accadia, M.; Piacentino, A.; Vicidomini, M. Thermoeconomic optimization of a renewable polygeneration system serving a small isolated community. *Energies* **2015**, *8*, 995–1024. [CrossRef]
24. Askari, I.B.; Calise, F.; Vicidomini, M. Design and comparative techno-economic analysis of two solar polygeneration systems applied for electricity, cooling and fresh water production. *Energies* **2019**, *12*, 4401. [CrossRef]
25. Tzivanidis, C.; Bellos, E. A comparative study of solar-driven trigeneration systems for the building sector. *Energies* **2020**, *13*, 2074. [CrossRef]
26. Heng, Z.; Feipeng, C.; Yang, L.; Haiping, C.; Kai, L.; Boran, Y. The performance analysis of a LCPV/T assisted absorption refrigeration system. *Renew. Energy* **2019**, *143*, 1852–1864. [CrossRef]

27. Yang, L.; Heng, Z.; Haiping, C.; Han, Y.; Fei, Y. Simulating and experimental research on a low-concentrating PV/T triple-generation system. *Energy Convers. Manag.* **2019**, *199*, 111942. [CrossRef]
28. Klein, S.A. Solar Energy Laboratory. In *TRNSYS*; A Transient System Simulation Program; University of Wisconsin: Madison, WI, USA, 2006.
29. Yang, S.; Li, H.; Yin, J. Development and Application of Frequency Conversion Pump Module Based on TRNSYS software. *J. HV AC* **2015**, *8*, 36–41.